Available online at www.sciencedirect.com

SCIENCE DIRECT®

Geomorphology 66 (2005) 215–235

GEOMORPHOLOGY

www.elsevier.com/locate/geomorph

Triggering conditions and mobility of debris flows associated to complex earthflows

J.-P. Malet[a,*], D. Laigle[b], A. Remaître[a], O. Maquaire[a]

[a]*School and Observatory of Earth Sciences, Institute of Global Physics, UMR 7516 CNRS-ULP, 5 rue René Descartes, F-67084 Strasbourg Cedex, France*

[b]*Cemagref - Snow Avalanche and Torrent Control Research Unit, B.P. 76, 2, rue de la Papeterie, F-38042, Saint-Martin d'Hères, France*

Received 9 December 2002; received in revised form 28 February 2004; accepted 15 September 2004
Available online 19 November 2004

Abstract

Landslides on black marl slopes of the French Alps are, in most cases, complex catastrophic failures in which the initial structural slides transform into slow-moving earthflows. Under specific hydrological conditions, these earthflows can transform into debris flows. Due to their sediment volume and their high mobility, debris flow induced by landslides are far much dangerous than these resulting from continuous erosive processes. A fundamental point to correctly delineate the area exposed to debris flows on the alluvial fans is therefore to understand why and how some earthflows transform into debris flow while most of them stabilize.

In this paper, a case of transformation from earthflow to debris flow is presented and analysed. An approach combining geomorphology, hydrology, geotechnics and rheology is adopted to model the debris flow initiation (failure stage) and its runout (postfailure stage). Using the Super-Sauze earthflow (Alpes-de-Haute-Provence, France) as a case study, the objective is to characterize the hydrological and mechanical conditions leading to debris flow initiation in such cohesive material.

Results show a very good agreement between the observed runout distances and these calculated using the debris flow modeling code Cemagref 1-D. The deposit thickness in the depositional area and the velocities of the debris flows are also well reproduced. Furthermore, a dynamic slope stability analysis shows that conditions in the debris source area under average pore water pressures and moisture contents are close to failure. A small excess of water can therefore initiate failure. Seepage analysis is used to estimate the volume of debris that can be released for several hydroclimatic conditions. The failed volumes are then introduced in the Cemagref 1-D runout code to propose debris flow hazard scenarios.

Results show that clayey earthflow can transform under 5-year return period rainfall conditions into 1-km runout debris flow of volumes ranging between 2000 to 5000 m^3. Slope failures induced by 25-year return period rainfall can trigger large debris flow events (30,000 to 50,000 m^3) that can reach the alluvial fan and cause damage.

Keywords: Earthflow; Debris flow; Modeling; Rheology; Runout; Hazard assessment

* Corresponding author. Now at: Faculty of Geosciences, University of Utrecht, The Netherlands.
E-mail address: J.Malet@geog.uu.nl (J.-P. Malet).

0169-555X/$ - see front matter © 2004 Elsevier B.V. All rights reserved.
doi:10.1016/j.geomorph.2004.09.014

1. Introduction

Mountain river valleys contain vast areas periodically exposed to catastrophic debris flows in case of strong meteorological precipitations or rapid snowmelt. This is particularly true for clay shales basins of southeast France known for their susceptibility to trigger muddy debris flows (Malet et al., 2004). These muddy debris flows are characterized by huge volumes of solid debris that are then deposited on alluvial fans. Schematically, these debris flows can initiate through two types of mechanisms. On one hand, initiation can occur in a torrential stream during an intense and localised thunderstorm after the concentration by runoff processes of loose material provided by shallow landslides affecting the watershed slopes or the breaking of a natural dam. On the other hand, initiation can occur through the liquefaction of slow-moving landslides experiencing a significant creep behaviour.

Classically, the transformation from a slide to a debris flow is depicted in three stages: (a) the failure localized along a surface within a creeping soil described using the Mohr–Coulomb plastic criterion; (b) the liquefaction of the bulk as a result of high pore water (fluid) pressure due to rapid infiltration in cracks; (c) acceleration and initiation of the debris flow. Presumably, as stated by several authors (Hungr, 1995; Iverson, 1997a; Iverson et al., 1997; Ancey, 2002), failure of the landslide mass is due to a combination of several mechanisms: rapid creep deformation, sudden increase in pore pressures and increase in load or erosion at the foot of the sliding mass. A high water content (higher than the liquid limit) is a necessary condition for the soil to be saturated and determines the liquefaction of the bulk. Saturation of the bulk causes intense surface runoff, complete saturation of the cracks and a sudden increase in the pore water pressures. Most debris flows occur during or after heavy and sustained rainfalls. In some cases, snowmelt can be sufficient to initiate debris flows, but for the remobilisation of unconsolidated landslide deposits, a combination of thawing soils, rainfall and snowmelt is often invoked. This is particularly true for impermeable clayey material.

Due to their sediment volume, debris flows induced by landslides are both far more dangerous than those resulting from continuous erosive processes and have an associated potential high hazard magnitude. In most cases, clayey earthflows experience significant creep behaviour (Picarelli, 2001), then decelerate and finally stop flowing after achieving a new hydromechanical equilibrium (Malet et al., 2004a). However, in a limited number of cases, earthflows may accelerate suddenly and give rises to debris flows. A fundamental point to correctly delineate the area exposed to debris flows on alluvial fans is therefore to understand why and how some earthflows transform into debris flow while most of them stabilize. As stressed by Crosta (2001), answering this question is difficult because it is the result of the action of several factors, such as (1) the hydrological and mechanical characteristics of the involved material, (2) the rapidity of the failure stage and postfailure stage (Vaunat and Leroueil, 2002), (3) the continuous changing of material properties (grain-size distribution, rheological characteristics) during flowing due to water feeding and channel-bed material scouring (Pierson and Costa, 1987; Hungr, 1995) or (4) the morphological characteristics of the flowing path (Hutchinson, 1988).

The Callovo–Oxfordian "Terres-Noires" of the Ubaye valley (southern Alps, France) are known for their numerous active landslides (Antoine et al., 1995; Maquaire et al., 2003). Three large earthflows (Poche, Super-Sauze and La Valette) have developed in this formation and have initiated more or less mobile mudflows or muddy debris flows in the recent years (LeMignon and Cojean, 2002), including a large range of volumes, for instance from 5000 to over than 60,000 m^3 at La Valette in 1988 (van Beek and van Asch, 1996). In this latter case, to prevent further catastrophic development on the urbanized alluvial fans, remedial measures were taken by the Service de Restauration des Terrains en Montagne, including groundwater drainage, displacements monitoring and the design of a sediment trap.

In this paper, two debris flow case histories of the complex Super-Sauze earthflow, representative of black marl landslides, are presented to evaluate the processes involved during the transition from failure to postfailure behaviour. The Super-Sauze earthflow affects the north facing slope of the Brec Second crest where the combination of steep slopes (up to 35°), downslope stratigraphic dip and the lack of vegetation make this basin one of the most landslide and debris

flow prone areas in the Ubaye valley. The earthflow has been studied since 1991 because of its entirely natural evolution (Maquaire et al., 2001).

It is important to notice that only small debris flow volumes have been released (from 5000 to 10,000 m^3) from the earthflow (750,000 m^3). Nevertheless, previous numerical analyses with the simple one-dimensional dynamic runout model BING have suggested that the release of larger volumes is a realistic option (Malet et al., 2004a). The main objective is to propose a methodology which aims at:

- assessing the conditions of stability of the debris source area to identify the hydrological conditions leading to debris flow initiation;
- assessing the rheological properties of the material in the debris source area to identify the material which presents the higher ability to flow for various total solid fractions;
- modeling the runout of these clay-rich debris flows assuming a viscoplastic flow type;
- simulating hazard scenarios to identify the volumes of sediment and water necessary to reach the alluvial fan.

2. The Super-Sauze landslide and its muddy debris flow events

2.1. Terminology of flow-like landslides

The classification of the flow-like landslides proposed by Hungr et al. (2001) is used in this paper to describe and distinguish the earthflow, mudflow and debris flow phenomena that appeared on the complex Super-Sauze landslide. Grain-size distributions of these landslides deposits show their muddy character (Malet et al., 2003a).

In this paper, the term earthflow refers to a slow to moderate (0.01 to 0.40 m day^{-1}) continuous flow-like movement of plastic clayey earth. The progressive weathering of the black marl produces a silty clay poorly sorted matrix with a consistency closer to the plastic limit than the liquid limit. Continued movement is maintained over long distances and periods of time by intermittent plastic deformation related to pore pressure fluctuations (Picarelli, 2001; Malet et al., 2002a). Earthflow material accumulates on the slope in a tongue-like form.

The term mudflow (0.1 to 1 m min^{-1}) refers to a rapid flow of saturated plastic debris in a channel or on the hill slope, involving significantly greater water content relative to the source material (slightly higher than the liquid limit). The matrix of the mudflow is often more cohesive than of debris flow. The gravel fraction is less represented. The runout distances of mudflows are often hectometric.

Finally, the term debris flow refers to a rapid shallow flow of partially or fully saturated debris in a steep channel The movement begins as a more or less surficial sliding failure on a scarp and continues to develop into a rapidly moving wave-like flow with velocities ranging from 1 to 4 m s^{-1}.

2.2. Characteristics of the study area

2.2.1. Geomorphological features of the Sauze catchment basin

The Super-Sauze earthflow (Alpes-de-Haute-Provence, France) has developed in the Roubines area, an enclosed marly torrential basin gullied in badlands (Fig. 1a). The Roubines area is located in the upper part of the catchment basin of the Sauze torrent, a tributary of the Ubaye river. The torrent watershed extends over 4.8 km^2 between 2685 and 1140 m in altitude for a length of 5.8 km. The flow regime of the torrent is characterized by high discharges in May and June due to snowmelt and by summer floods caused by cloudbursts. Floods may also occur in autumn, but the catchment elevation is such that precipitation generally occurs as snowfall. The Sauze drainage basin is characterized by an upper rock basin consisting of limestone formations partially covered by moraine tongues, whereas the median and downstream parts are cut into the black marl.

The torrent has a length of 3.4 km from the base of the debris source area to the apex (Fig. 1a) for slopes ranging from 4° to 35°. The distance from the apex to the confluence with the Ubaye river reaches 1.2 km for an average slope of the fan of 4°. If the upstream part of the basin is characterized by the absence of vegetation, the median and downstream parts are forested and covered by moraine deposits varying in thickness between 0.3 and 3.5 m. Much of the channel

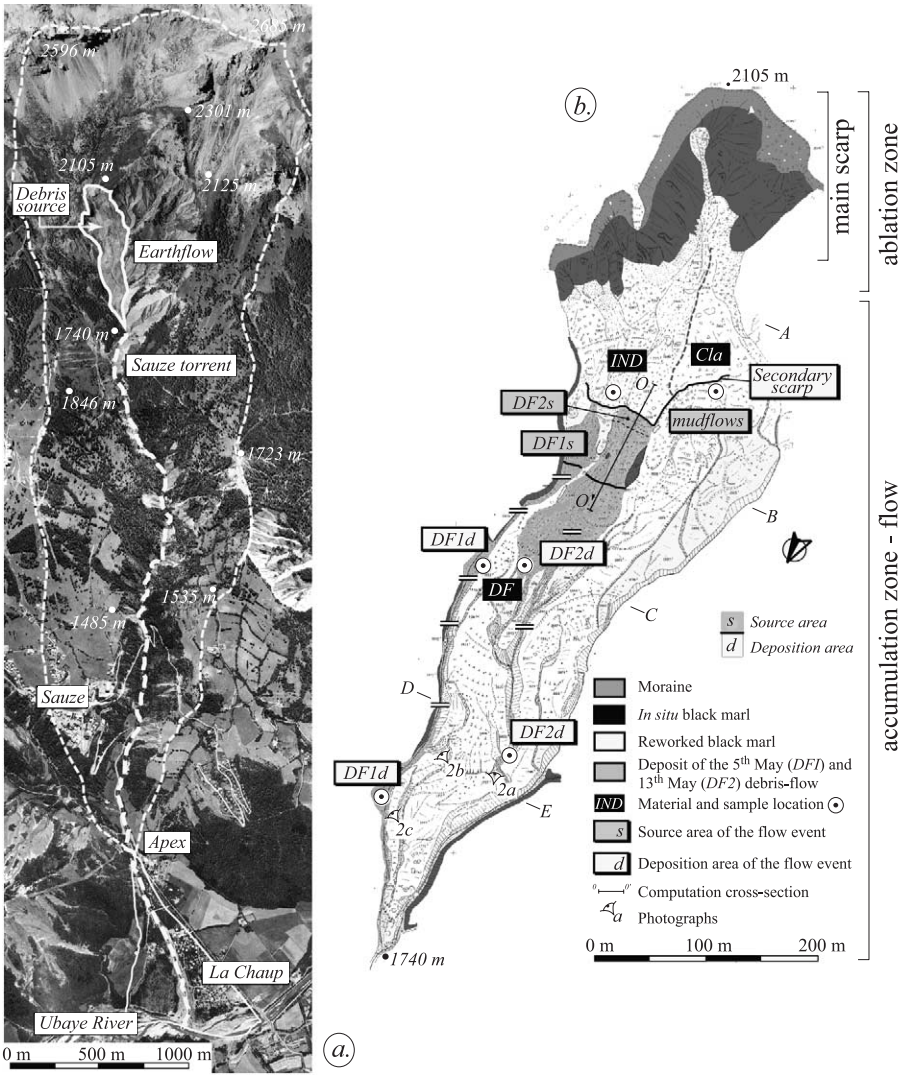

Fig. 1. Orthophotograph of the Sauze catchment (a) and morphological map of the Super-Sauze earthflow (b).

has steep slopes ranging between 28° and 40°. Only the badland areas reaching the channel are susceptible to surficial landslides and runoff erosion processes.

The alluvial fan is highly urbanized (housing development of La Chaup and commercial services, Fig. 1a) and therefore exposed to debris flow hazard.

2.2.2. Geomorphological and geotechnical features of the Super-Sauze earthflow

The Super-Sauze earthflow is located in the headwater basin between 2105 (crown) and 1740 m (toe of the flow) for an average slope of 25° (Fig. 1b). The earthflow covers a 0.17 km^2 surface (length, 0.8 km; maximum width, 0.2 km) for a thickness ranging between 8 and 20 m.

Although apparently unaffected in the 1950s, the area suffered falls of blocks and structural slides in the 1960s. The progression of a flow in the 1970s progressively buried a torrential channel (Maquaire et al., 2001). Uphill, the main scarp inclined at approximately 70° cuts into moraine deposits and subjacent in situ black marl steep slopes about 100 m high. Below the main scarp, the so-called "upper shelf" (Fig. 1b) appears as a block field, with black

marl slabs more or less buried in a very heterogeneous reworked formation. This latter formation is a fine silty matrix containing pebbles and crumbly flakes with a consistency closer to the plastic than the liquid limit. Progressing downstream, an area of dislocated and disintegrating blocks passes to an uneven rough surface of crumbling blocks and, finally, to a slightly uneven surface scattered with calcite and moraine pebbles, weathered marly stones and flakes of various sizes. The intermediate slopes on this section range up 20° to 25°.

Geotechnical investigations, inclinometric measurements (Flageollet et al., 2000) and geophysical prospecting indicate that the channelized flow buries a complex topography (Maquaire et al., 2001) formed by a succession of parallel crests and gullies. The flow consists of two superimposed units. The upper unit, 5 to 10 m thick, is a very active and very wet viscous muddy formation, while the lower with a maximum thickness of 10 m is a stiff compact, impervious and stable formation (Malet et al., 2002a). The total volume is estimated at 750,000 m^3. The earthflow exhibits a macroviscous behaviour, with a wide range of velocity which varies with time (from 0.01 to 0.40 m day^{-1}). Field observations and measurements show that the movement may be maintained over long distances and for long periods of time by intermittent plastic deformations accompanied by the built-up of interstitial pore water pressures. These sudden groundwater table rises involve accelerations of the flow (Malet et al., 2002a). The upper unit can trigger rapid flow-like phenomena, such as in spring 1999 when two muddy debris flows and a dozen small mudflows occurred.

2.3. The muddy debris flows events of Spring 1999

2.3.1. Morphological and kinematical features of the muddy debris flows

On 1999, May 5 (12:10 a.m. GMT), a volume of material (DF1) failed suddenly from the secondary scarp, flowed rapidly down the hill slope and reached the eastern torrent flanking the earthflow (Fig. 1b, area $DF1_d$). The peak velocity estimated by the forced vortex equation (Johnson and Rodine, 1984; Hungr et al., 1984) on five cross-sections (Fig. 1b) reached values of, from upstream to downstream, 3.8, 4.9, 5.1, 4.7 and 4.1 m s^{-1}.

During the night of 1999, May 12–13, a larger volume of material (DF2) failed in the same area. The material flowed along the same path as DF1 and channelized finally in the main central gully of the earthflow. The maximum velocity estimated from three cross-sections (Fig. 1b, area $DF2_d$) reached 3 m s^{-1} upstream and 2.8 m s^{-1} downstream.

In both cases, deposits are shallow flat-topped lobes with convex sides, becoming progressively more sheet-like in the downward direction. The thickness of the deposits reach 1.2 to 1.6 m for DF1 and 1.9 to 2.6 m for DF2. Lateral sorting is poor, whereas vertical rough sorting is high. The coarser clasts and boulders are concentrated at the top of the flow surface (Fig. 2c). The dried deposit is characterized by strong cohesion. Due to the specific morphological conditions, most of

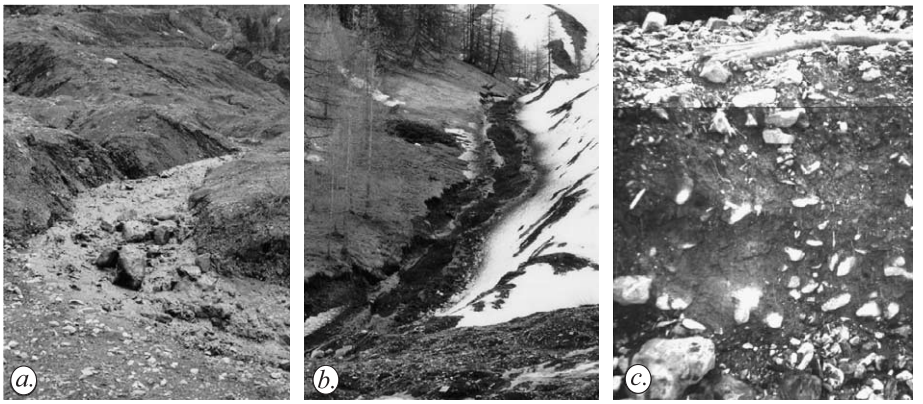

Fig. 2. Photographs of the runout of the muddy debris flows DF2 (a) and DF1 (b). Photograph of the stratigraphy of debris flow DF2 in the depositional area (c).

the materials involved came to a stop on the lower shelf of the earthflow, and only a small proportion reached the torrent bed at the toe of the earthflow. A detailed morphological description of the debris flow events can be found in Malet et al. (2003a, 2004).

A detailed morphologic mapping of the deposits and the comparison of two DEMs before and after the events (Henry et al., 2002) allowed the volumes of the events to be estimated at 2500 m^3 for DF1 and 7700 m^3 for DF2. The two events were triggered from the secondary scarp of the earthflow (Fig. 1b) as rotational slides, but they acquired flow characteristics very quickly. A significant surface was eroded inasmuch as the height of the secondary scarp passes from 5 to 12 m after the failures. The failed material was totally saturated. This is supported by observations of abundant springs appearing within the unstable area during the preceding days, as well as a rise in groundwater levels.

After these two events, mudflows of varying size were observed in the western part of the initiation area at the base of the secondary scarp (Fig. 1b). These mudflows travelled 100 to 250 m on the earthflow with slower velocities (0.5 to 1 m min^{-1}; Malet et al., 2004a).

2.3.2. Meteorological and hydrological conditions

Hydrological data were obtained from the rain gauge of Super-Sauze (1750 m a.s.l.) located about 800 m from the earthflow. An average value of 734 mm can be considered typical of this Mediterranean mountainous climate characterized by highly variable rainfall (400 to 1300 mm $year^{-1}$), intense summer and autumn storms (reaching potential intensities of 50 mm h^{-1} in 15 min) and on average 130 days $year^{-1}$ of freezing. Rainfall occurs mainly in the autumn (maximum value of 278 mm in October, minimum value of 5 mm in July). The average monthly temperature is at its highest in July–August (12.7 °C) and lowest in December–January (−1.7 °C). Snow cover is also highly variable at 2000 m and ranges between 0.3 and 2.7 m (Malet, 2003).

If the effective accumulated rainfall on 13 May 1999 (233 mm) corresponds to the average value of the period 1991–2001, the rainfall distribution over the period January–May is very different. The precipitation falling over the period 15 April–13 May amounted to more than 50% of the precipitation since the beginning of the year (Fig. 3a). The total precipitation can be divided into two meteorological events: ME1, 67 mm from 19 to 27 April, 10 days before the onset of DF1, and ME2, 71 mm from 2 to 7 May and 51 mm from 2 to 5 May. A detailed statistical–hydrological analysis of the continuous sequence of available rainfall data was performed to understand if the characteristics of the hydrological event triggering the DF1 debris flow were exceptional.

The distribution function Generalized Extreme Value (Jenkinson, 1955) has been calculated on the annual maximum cumulative rainfall values (1, 3, 6, 12 and 24 h and 2, 3, 5, 10, 20, 30, 45, 60 and 90 days) to estimate the return time, following the procedure described by Fiorillo et al. (2001). The results for the return times of the cumulative rainfall recorded at the onset of the DF1 event are shown in Fig. 3b. Return times increase gradually up to the cumulative rainfall of 3 days and decrease slowly for higher number of days. If the rain in the 3-day period preceding the onset is specific, it can not be considered exceptional because the return time for a 51-mm cumulative rainfall in 3 days is 6 years. The exceptional character of the hydrological event is therefore related to the combination of rainfall and snowmelt.

For DF2, the trigger is related only to snowmelt, as no rainfall had occurred (Fig. 3a). Indeed, the winter 1998/1999 appears to have been exceptional in term of snow cover. At 2000 m, snow cover varies between 2.0 and 2.2 m over the period between 31 January and 31 March, which is the highest value inasmuch as snow depth is measured at the Super-Sauze ski resort (1986). Moreover, high snowfalls occurred also in February, March and April, while snowmelt appeared very late (in contrast to the previous years). At the end of March, snow cover reached 2.2 m (compared with 1.3 m in March 1997 and 0.6 m in March 1998).

The exceptional character is also related to the daily temperature variations, which indirectly allows estimates of the snowmelt rate. Thus, a spectacular rise of temperature was observed during 18 continuous days, with the daily mean temperature rising from 2 °C on 25 April to 18 °C on 13 May (i.e., an increase of 0.8 °C/day). Such an increase has never been recorded in the temperature times series. In combination to the precipitation events, this rise involved a fast snowmelt above 1850 m a.s.l. from 1 May (Malet, 2003).

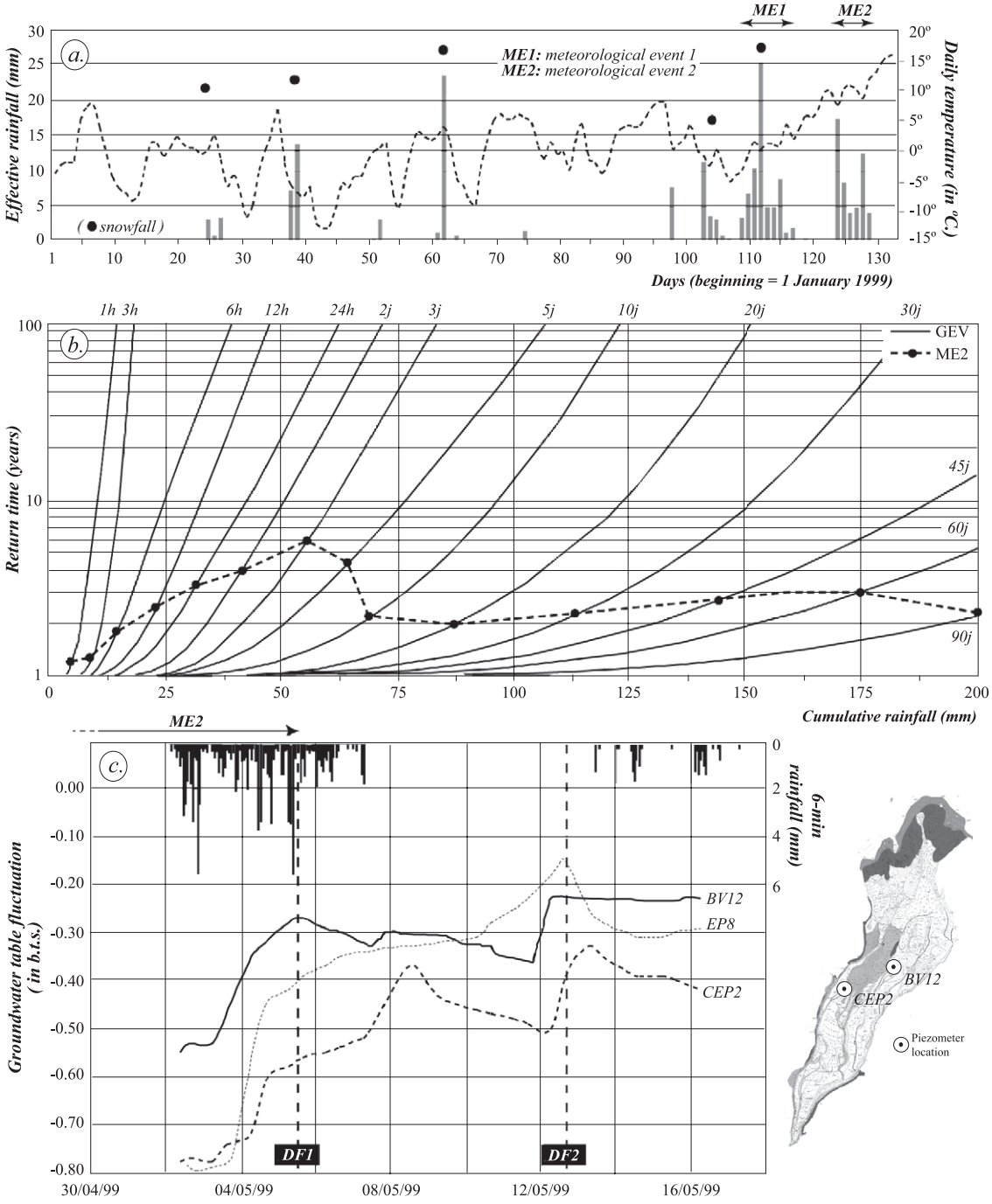

Fig. 3. Hydrological conditions leading to the observed muddy debris flows events. Effective daily rainfall and temperature at 1900 m (a.s.l.) over the period 01/01/1999 to 13/05/1999 (a). Return time cumulative rainfall from generalized extreme value distribution (b). Rainfall, groundwater table fluctuations, onset of debris flow relationships and piezometer location on the earthflow (c).

This combination of precipitation and rapid snowmelt explains the significant increase of the groundwater level on the uphill cross-sections (A, B, C) where the average level reaches approximately 0.30 m below the topographic surface (Fig. 3c). A sudden increase in groundwater levels occurred on 4–5 May near the initiation zone. Approximately 18 h after the initiation of DF1, an increase also occurred on the C cross-section. Another abrupt increase occurred on 12 May before the onset of DF2.

From these observations, it appears that the failure mechanism can be attributed to a sudden rise in pore water pressure, and that the failed material is nearly completely saturated far beyond the plasticity limit of the material and near the liquid limit. Therefore, an important question to answer is whether or not the (upper part) of the earthflow can partially or totally transform itself into an important debris flow. The potential for generating a large volume event will depend upon (1) the mechanical properties of the involved material, (2) the stability conditions of the source area and (3) the ability of the debris to runout along the torrent.

3. Approach and methodology

The following analysis uses a geomorphological terminology for describing the main sections along a flow (Hungr et al., 2001): the source area (which refers to the starting zone of the material), the transport zone and the depositional area. From a geotechnical and rheological point of view, we also use the terms "prefailure," "failure" and "postfailure" to describe the various stages of the events (Vaunat and Leroueil, 2002). The differences in the runout distances of the observed deposits can be explained in terms of either the rheological properties of the earthflow material, the release volume or the flow mechanics of the debris. To address the above questions, a four-step analysis was followed (Fig. 4): (1) a characterization of the hydrological, geotechnical and rheological properties of the material, (2) a seepage analysis to define the hydrological conditions governing the prefailure stage, (3) a limit equilibrium analysis of slope failure conditions and, finally, (4) an estimation of runout scenarios for different failed masses with the Cemagref 1-D debris flow runout model.

The rheological properties of the failed mass determine the response of the debris to external and internal forces, such as bed friction, surface stress, internal shear and gravity (Takahashi, 1991). They were determined at the laboratory scale by coupling rheometrical tests and inclined plane tests (Malet et al., 2003a) and at the field scale through the analysis of the shape of the deposits at stoppage (Coussot et al., 1996).

The amount of material mobilized in the failure stage (release volume) influences runout distances.

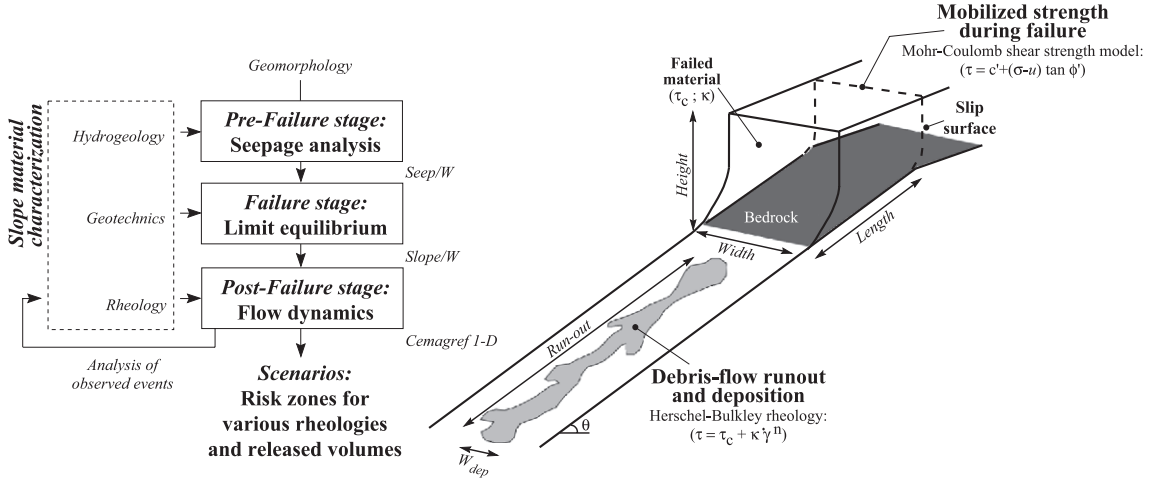

Fig. 4. Approach used for defining the various stages of the landslide event and conceptual model illustrating the generation of debris flows from the Super-Sauze earthflow.

This behaviour has been observed for subaerial debris flows (O'Brien et al., 1993; Iverson et al., 1997; Ancey, 2002), subaqueous debris flows (Suhayda and Prior, 1979; Edgers and Karlsrud, 1982; Locat et al., 1996), rockslides (Heim, 1932; Scheidegger, 1973) and snow avalanches (Harbitz et al., 1998). Hence, it is worth noting that several debris flow studies (Irgens and Norem, 1996; Rickenmann, 1999; Klubertanz et al., 2000; Iverson, 2003) reveal that lower slope environments normally permit more material to be accumulated before release resulting in larger and less frequent events. This suggests that failures of the upper part of the Super-Sauze earthflow characterized by a large flat area (the "upper shelf") behind a secondary scarp can result in larger failures than on a landslide marked by a constant slope.

For the prefailure and failure stages, transient computer simulations were carried out to evaluate the stability of the source area in unsaturated conditions. The modeling was carried out using the two-dimensional finite-element model SEEP/W (Geo-Slope, 2000) which adopts an implicit solution scheme to solve Richard's equation for saturated and unsaturated conditions (Richards, 1931). Calculations are based on eight-noded quadrilateral elements. Output is produced in the form of steady-state positive and negative pore water pressures and volumetric moisture content. The pore water pressures (positive and negative) were then used as inputs to the slope stability model SLOPE/W (Geo-Slope, 2000) to assess the limit equilibrium state of the slope under ambient and critical pore water pressures. The governing parameter for slope stability is the Mohr–Coulomb shear strength τ mobilized along the failure plane, which is dependent (Lambe and Whitman, 1979) on the internal angle of friction ϕ', the cohesion c' (if any) and the effective stress (defined as the difference between the total normal stress σ_n and the pore pressure u):

$$\tau = c' + (\sigma_n - u)\tan\phi'$$

(Mohr − Coulomb strength model)

For postfailure analysis, the flow dynamics model Cemagref 1-D developed by Laigle and Coussot (1997) for the study of the downslope runout of finite source muddy debris flow was used. The model computes unsteady free-surface flows of viscoplastic mud, and the flow is assumed to remain laminar and incompressible throughout the computation. The code uses a one-dimensional formulation for an Herschel–Bulkley constitutive equation. In the Herschel–Bulkley rheology, the mud is considered to consist of a distinct shear layer and a plug layer (Herschel and Bulkley, 1926). The shear stress at the interface of these two layers is the yield stress. The material can deform only if the applied stress exceeds the yield stress. Therefore, the model is theoretically valid only for muddy flow-like landslides with at least 10% of clay particles. Considering that the muddy debris flows observed at Super-Sauze exhibit yield stress due to interactions between clay particles and are generally shear thinning, the model of Coussot (1997) is well adapted to describe such behaviour. For simple shear conditions, the shear stress–shear rate ($\tau-\kappa$) relationship (shear stress, τ; shear rate, γ; yield stress, τ_c; shape parameter or consistency, κ; power law exponent assumed to be equal to 1/3, n) is written as follows:

$$\tau = \tau_c + (\kappa \cdot \gamma^n)$$

(Herschel − Bulkley viscoplastic model for yield stress fluids)

The three rheological parameters are implemented in the code as two ratios (κ/τ_c, τ_c/ρ) both to ensure numerical stability and to limit the number of variables. A discharge hydrograph is required to set the total volume of the event.

The governing equations describing the conservation of mass and momentum are solved in a traditional Eulerian framework with a fixed grid system. In the numerical scheme, the motion of the material for a muddy debris flow is represented with a moving one-dimensional system of equations usually referred to as the steep slope shallow water equations. The number of grid cells remains the same throughout the calculation. Each grid node is allowed to move at the local depth-averaged velocity after each time step. Resolution of the differential equations is based on a Godunov-type explicit numerical scheme. The width normal to the flow is variable and a function of two morphological parameters (K, α) which allow representing the geometry of the channel. Therefore, the

model accounts for depths changes due to widening/narrowing of the channel bed path.

As outputs, the Cemagref 1-D code calculates the flow thickness in the wet perimeter, velocity and discharge. The equations of motion and the numerical scheme are detailed in Laigle and Coussot (1997). Sensibility of the model is described in Malet et al. (2004b).

4. Characterization of the earthflow material and the muddy debris flow deposits

Grain-size analyses, Proctor compaction tests, bulk and dry density tests and consistency limit tests have been performed on the earthflow material together with a mineralogy analysis, permeability tests and direct-shear strength tests. Analyses have been carried out on undisturbed samples collected (Fig. 1b) on the secondary main scarp (IND), on the western slope area (C1a) and in the deposits of DF1 and DF2 events.

4.1. The debris source area

All the materials are relatively homogeneous from a mineralogical standpoint, mainly composed by illites, chlorites and kaolinites. No swelling clays were detected. The deposits contain a maximum of 25–30% of coarse (gravel) material although protruding boulders of up to 4 m in diameter can be coated in the mud. On the basis of some 30 analyses on the fraction passing the 20-mm sieve, all matrix samples have a high content of silt and clay (more than 60% of sand, silt and clay and more than 25% of clay and silt) and the textural classes range from silty clay for material C1a to silty sand for IND. Finally, the grain-size distribution (Fig. 5a) of the two debris flow deposits DF1 and DF2 can not be distinguished and are identical to those of the secondary scarp (IND). This indicates that the debris source material has undergone very little modification during the runout inasmuch as the grain-size envelopes are very close. All the material can be defined as cohesive (Coussot and Meunier, 1996; Hungr et al., 2001).

Dry unit weights lie in the range 1200 to 1760 kg m^{-3} as saturated unit weights lie in the range 1700 to 2140 kg m^{-3}. Results obtained from modified Proctor tests on the fraction <20 mm indicate a maximum dry density between 1830 and 1920 kg m^{-3} and an optimum moisture content between 9.3% and 12.4%. The IND formations show a more fragile behaviour during changing moisture conditions. Atterberg consistency limits (Fig. 5b) classify the material as inorganic clays with low plasticity (I_p=13–16).

Soil conductivity was extensively tested both in laboratory (constant and falling head permeameter)

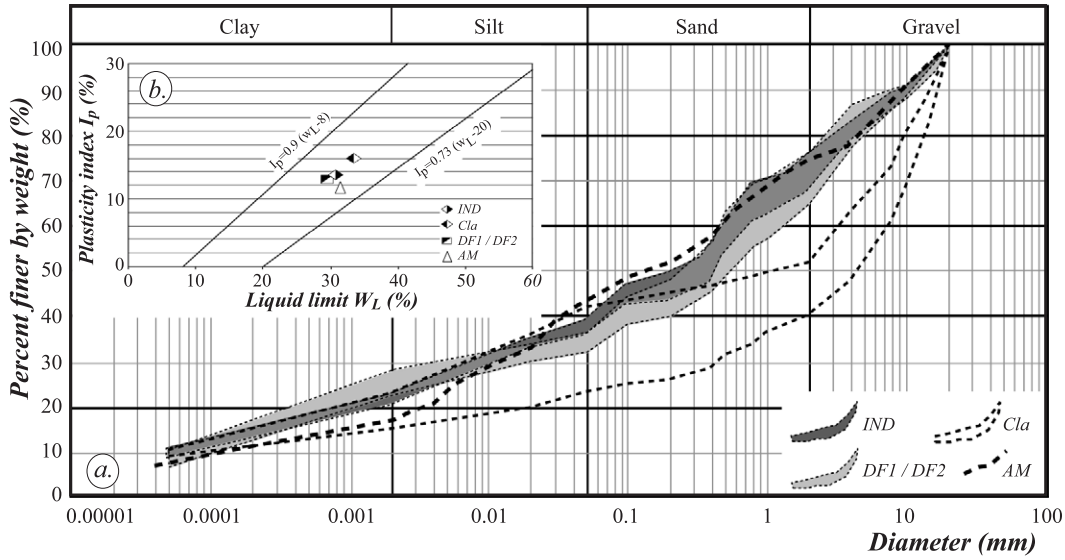

Fig. 5. Grain-size distribution envelopes (a) and Casagrande diagram (b) for the different materials.

and in situ (auger hole tests, tension disk infiltrometer) under pressure or suction (Malet et al., 2003b). The conductivity values classify the material as semi-permeable and are in direct connection with the grain-size distribution of the formations; C1a presents one order of magnitude lower average saturated conductivity values ($1.4\ 10^{-6}$ms^{-1}) than IND ($1.8\ 10^{-5}$ ms^{-1}). The presence of deep and frequent cracks on the secondary scarp can result in higher effective conductivity values (Malet et al., submitted for publication). Finally, some direct-shear strength tests were carried out using a Casagrande apparatus on undisturbed samples (Maquaire et al., 2003). Clearly, no cohesion was present, and an average friction angle of 28° was measured. IND shows a lower friction angle (26–29°) than C1a (29–32°).

The geotechnical characteristics of the debris source area and of the debris flow deposits are very similar; moreover the material of the debris source area exhibits lower strength characteristics than the other part of the earthflow. To estimate the proportion of black marl and moraine in material IND, several artificial mixtures were prepared and compared (Malet et al., 2003a). The artificial mixture AM composed of 30% moraine and 70% marl presents the same texture and consistency characteristics as IND.

4.2. Rheological characteristics of the debris source area and the debris flow deposits

Rheological parameters influence the outputs of the runout models significantly (Rickenmann and Koch, 1997). The direct determination of the behaviour of flow material with the help of rheometers is faced with the irretrievable problem that they generally contain particles of various sizes, including big boulders (Coussot and Meunier, 1996). Numerous studies have demonstrated that the behaviour of fine-grained flows is mainly guided by the muddy matrix, which acts as a lubricant rather than the blocks or debris carried (Pierson and Costa, 1987; O'Brien and Julien, 1988; Major and Pierson, 1992; Coussot and Meunier, 1996). At the opposite, in the case of coarse-grained flows where rheology evolves as mixture agitation, grain concentration and fluid pressure change during flow initiation, transit and deposition (Iverson, 1997b; Iverson and Vallance, 2001), simple constitutive relations (Bingham, Herschel–Bulkley) are not able to capture the complex grain–grain and water–grain interactions controlling these flows. We therefore carried out a rheological characterization of the material by parallel plate rheometry on the <400-μm fraction by inclined plane tests on the <20-mm fraction and by analysing at the field scale the shape of the deposit at stoppage by using the relation proposed by Coussot et al. (1996), taking into account the asymptotic flow depth and the shape of the lateral levee. Due to limitations in the experimental devices, the range of shear rates γ (0.02 to 18,700 s^{-1}) used in this study is two to three times higher than that met with this type of flow in the field (O'Brien and Julien, 1988). A detailed analysis of the rheological properties (Table 1) can be found in Malet et al. (2002b, 2003a).

All the materials exhibit a viscoplastic behaviour over the range of shear rates in consideration, well represented by a Herschel–Bulkley constitutive equation. Herschel–Bulkley parameters (τ_c, κ) increase with the total solid fraction. For total solid fractions between ϕ=0.30 and ϕ=0.60, the yield stress may vary by as much as three times, while the consistency varies only by twice as much (Fig. 6).

Laboratory results are consistent with those estimated at the field scale by the shape of the slurries at stoppage (Table 1). The differences are comprised between the margin of error specified by Coussot and Ancey (1999) who indicate that the difference in the yield stress estimation using several methods is between 10% to 25%. Nevertheless, yield

Table 1
Rheological properties of the debris source area material and of the muddy debris flow deposits for ϕ=0.45

	Rheometry			Inclined plane	Deposit shape
	τ_c	κ	n	τ_c	τ_c
	Pa	Pa s	/	Pa	Pa
C1a	182	120	0.31	211	/
IND	103	84	0.30	126	/
DF1	84	52	0.32	89	132
DF2	75	41	0.35	93	146
AM	142	86	0.29	168	/

τ_c is the yield stress; κ is the Herschel–Bulkley shape parameter or consistency; n is the power law exponent; ϕ is the total solid fraction.

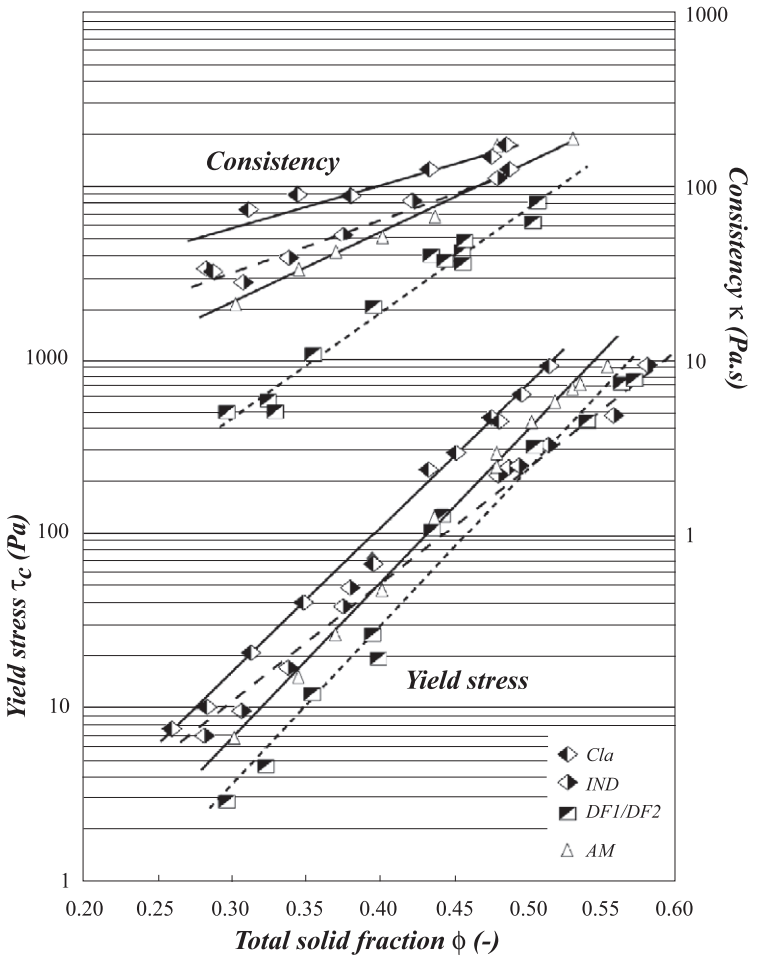

Fig. 6. Variation of the rheological properties (yield stress, τ_c, consistency, κ) as a function of the total solid fraction, using the rheometrical tests and the inclined plane tests. The yield stress is read on the right vertical axis, the consistency on the left vertical axis.

stress values and consistency values estimated by rheometry are somewhat lower than those based on field observations due to both a higher shear rate and experiments carried out on the <400-μm fraction.

Rheological parameters clearly distinguish two types of material in the debris source area: the cohesive silty clayey matrix (C1a) present high yield stress and viscosity and the sandy silty matrix (IND) present lower rheological characteristics (Fig. 6). This means that a higher volume of water is necessary to initiate a fluid behaviour in C1a material than in IND material. Combined with the hydrological and geotechnical characteristics, it appears that the main potential source of debris is therefore the eastern part of the secondary scarp cut in the IND material (Fig. 1b). The geometrical and morphological characteristics of this zone being also favourable to the release of debris, it is important to define the stability conditions of this zone.

5. The prefailure and failure stages

Laboratory data and field observations have been used to study the initial stability of the scarp and to forecast the potential volume of debris able to fail for given hydrological conditions. Prefailure and post-failure stability analyses have been performed by limit equilibrium methods. Analyses were based on the prefailure and postfailure topographic data derived

from two high-resolution DEMs (Henry et al., 2002). For slope stability analyses of the prefailure slope, the strength characteristics of the IND material (Table 2) and the geometry presented on Fig. 7a were used. For dry conditions, the slope is in equilibrium with a factor of safety (F_s) near 1.70; the potential instability factor is the generation of high groundwater levels (Fig. 3c) leading to excess pore water pressures.

Therefore, a parametric seepage analysis has been conducted to define the influence of pore water pressures and the mechanical effect of cracks on the overall stability of the debris source area. The seepage analysis was used to generate pore pressure distributions that were subsequently imported into limit equilibrium analyses. For the analysis, the slope was considered isotropic and homogeneous. The initial pore water distribution is derived from piezometers recordings before failure (Fig. 3c) and from continuous water tension measurements by fast-response and pressure transducer-based tensiometers (Malet, 2003). Consequently, total hydraulic heads and degrees of saturation are defined at all nodes. The groundwater flow regime is assumed to be acting two dimensionally along the cross-section being examined (Fig. 7a, b). Another assumption is that hydraulic conductivity of the material ($1.8\ 10^{-5}$ ms^{-1}) is the same in the vertical and horizontal directions. Boundary conditions were assigned in such a manner as to generate a water table in the upper part of the slope and create downward flow towards the toe. Zero flow boundary conditions were implemented on the bottom and left boundaries to represent an impermeable layer at the base (Fig. 7b). On the right side, a constant head boundary equal to the height of the depth to the impermeable base was established. Seepage faces were assigned to the slope itself and the ground surface at the toe of the slope. To generate groundwater and, hence, a water table, a flux was specified on the top of the slope. Simulations were performed using a meteorological event of 6-year return period corresponding to the amount of water leading to the initiation of DF1.

Fig. 7b shows the total head distribution assuming an uncracked scarp. Results show that drainage from the scarp prevents the build up of high positive pore water pressures in the potential slide area. In every case, suctions of −5 kPa were maintained. The water table remains in this state until the rain ceases, whereupon it declines. This is in accordance with the presence of springs at the base of the scarp.

A Morgenstern–Price-type slope stability analysis was then carried out to evaluate the F_s of the scarp in this state. Analyses have been performed assuming a quasi-vertical slide surface upward and a more or less circular slide downward (Fig. 7a) as observed on the field. In each case, an analysis of over 300 slip searches was carried out to find the shear surface with the lowest F_s. Shallow surficial slides were eliminated by defining a minimum sliding depth of 2 m using the tangent straight line definition. The results (Fig. 7g) highlight the importance of the unsaturated state on the overall stability. It is assumed here that the difference in F_s is of more interest than the actual value. The F_s is 1.45 where the field and computer simulation suctions are used and 1.15 if the effects of suction are ignored, and a pore water pressure of zero is assumed to exist above the water table. Suction must therefore be incorporated in the simulations inasmuch as they can lead to serious underestimation of F_s.

Field observations show that the debris source area is densely cracked. To investigate the mechanical effect of these cracks, simulations were performed with cracks of varying depth (0.8, 1.5 m) or location behind the scarp (10, 20, 30 m). Vertical cracks are

Table 2
Geotechnical characteristics of the tested material

	Grain size				Unit weight		Strength properties		Consistency		
	Sand (%)	Silt (%)	Clay (%)	Gravel (%)	ρ_d (kg m^{-3})	ρ_{sat} (kg m^{-3})	c' (kPa)	ϕ' (°)	W_P	W_L	I_p
C1a	25	22	15	38	1760	2140	16–37	29–32	16	32	16
IND	31	29	10	30	1220	1790	21–40	26–29	17	33	16
DF1/DF2	35	24	9	32	1200	1703	8–21	25–30	15	30	15
AM	29	35	10	25	/	/	/	/	18	31	13

ρ_d is the dry unit weight; ρ_{sat} is the saturated unit weight; c' is the effective cohesion; ϕ' is the effective internal angle of friction; W_P is the plasticity limit; W_L is the liquid limit; I_p is the plasticity index.

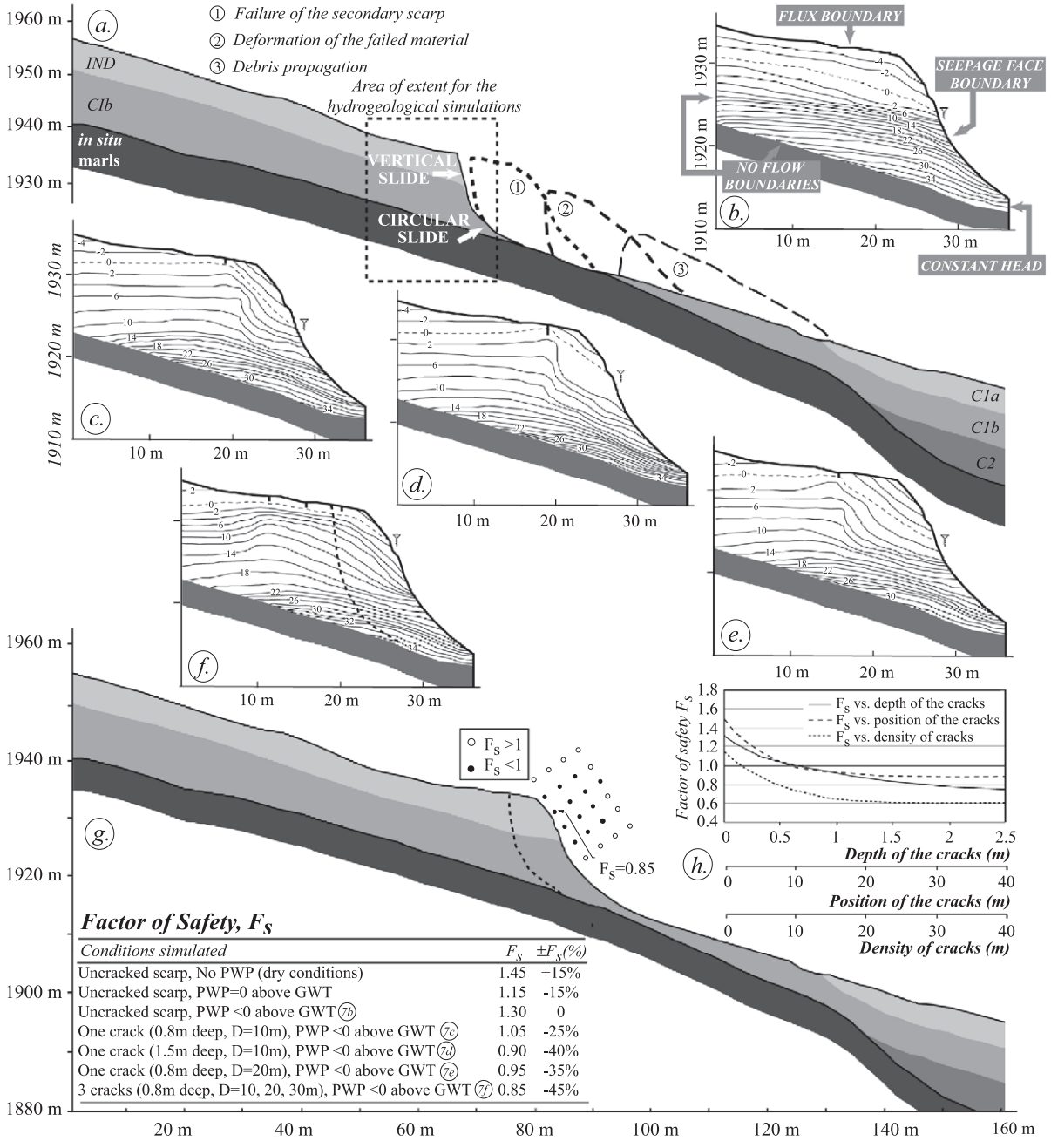

Fig. 7. Seepage and stability analyses of the debris source area. Cross-section showing the prefailure and postfailure observed morphological profiles and the progressive flowing of the mass (a). Simulated pore water responses to a 6-year return period meteorological event in an uncracked head (b) and for several cracked situations (c–f). Results of the combined seepage and stability simulations and location of the potential slip surface (g). Parametric analysis of the influence of cracks (h).

implemented in the model through specified tension crack lines of varying size corresponding to zones of increasing hydraulic conductivities.

As can be seen, the hydrological effect is very significant (Fig. 7c–f). For all simulations, the groundwater table reaches the topographic surface in some places, and pore suctions of −5 kPa are replaced by positive pressures of 2–8 kPa in the potential shear zone. Similar developments of positive pore pressures was also noticed by Collinson (2001) in marly gully heads of southeast Spain.

Appearance of the resulting water tables and equipotential lines for all cracked cases is fairly different than that for the uncracked cases. If the equipotential lines are approximately horizontal in the upstream part of the slope, indicating that flow is generally vertical, they curve up from the base of the scarp towards the surface in the downstream part of the slope. Velocity vectors show uniform velocity in the unsaturated zone above the water table increasing slightly into the saturated zone towards the bottom of the scarp. The velocity vectors indicate downward flow at the top of the slope and left to right within the slope. On the scarp, large velocity vectors occur where water is flowing out of the slope. Small flows are present below the scarp due to low gradients developed as a result of the boundary conditions imposed on the right.

The presence of cracks reduces F_s from 1.30 for uncracked conditions to 1.05 for a 0.8-m-deep crack located 10 m behind the scarp (Fig. 7c, g) and 0.90 for a 1.5-m-deep crack (Fig. 7d, g). The parametric analysis (Fig. 7g, h) demonstrates that the depth of cracks (Fig. 7c, e, g) and the number of cracks have a more important impact on reducing F_s than the position of the crack. A depth of crack larger than 1.5 m, a location at least 20 m behind the scarp and a density of cracks larger than 15% have little additional impact on F_s reduction (Fig. 7g). Therefore, assuming constant rainfall conditions, the reduction of F_s is largely a hydrological effect. The dominant process seems to be fissure flow in cracks nearby the scarp face, acting as a rapid water pathways to depth and causing excess pore water pressures (Malet, 2003).

Fig. 7g shows the position of the slip surface for the lowest F_s (F_s=0.85) assuming the presence of three 0.8-m-deep cracks, respectively, located 10, 20 and 30 m behind the scarp. These conditions are the closest to those observed before the triggering of DF1. The slip surface is located 7 m behind the scarp similar to that observed after the failure.

The performed stability analyses showed the crucial role played by partial saturation of the material and the influence of cracking. For various field conditions, simulations suggest that the debris source area is unstable, and that larger volumes of debris can be released for larger cumulated rainfall. The failed mass is nearly completely saturated and moves more or less as a single mass.

6. The postfailure stage

Before predicting the mobility of the failed debris to assess the hazard on the alluvial fan, we need to evaluate if the Hershel–Bulkley rheology and the Cemagref 1-D code are able to replicate field observations.

A sensitivity analysis of the model has demonstrated that the rheological parameters have a great influence on the modeling results (Laigle and Marchi, 2000; Malet et al., 2004b). For instance, a variation of 50% of τ_c/ρ values leads to a mean change of 50% on the deposit thickness, while a variation of 50% of κ/τ_c introduces changes up to 20% (Fig. 8a). Moreover, the effect of the rheological parameters depends on local slope gradients and discharges values. Consequently, the relative influence of the rheological parameters may not be the same for every debris flow event even if τ_c/ρ seems to be usually dominating. Some variations of the discharge values do not highly influence the deposit thickness even with a considerable increase imposed. At the opposite, the sensitivity of the model to variations of the input volume is important and significant for a volume variation of only 10% (Malet et al., 2004b). Influence of the geometrical parameters (slope gradient, shape parameters of the channel) on the computed deposit thickness are less sensitive; for instance, a variation of the slope angle of 20% leads to a mean change of 10% of the deposit thickness (Malet, 2003). Finally, model outputs are insensitive to the mesh configurations; a variation of the mesh size of 15% leads to an error on the theoretical computed velocity of less than 5% (Malet, 2003).

According to these results, the performance of the runout model has been evaluated by analysing the

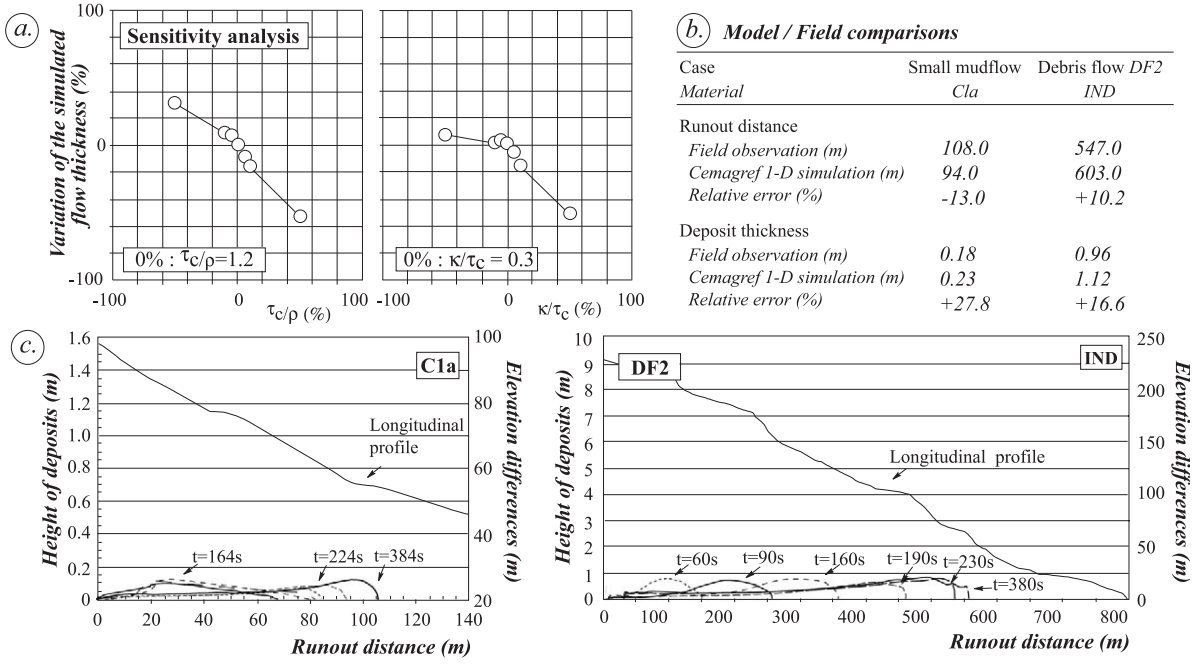

Fig. 8. Mobility analysis of a mudflow and a muddy debris flow. Sensitivity analysis on the simulated flow thickness with the influence of τ_c/ρ values and κ/τ_c values (a). Numerical simulations and field observations comparisons for the two case studies (b). Evolution of the geometry during propagation and final deposit shape (thickness, runout) at stoppage (best fit simulation) for the C1a mudflow (c) and the DF2 muddy debris flow (d).

mobility of a small mudflow initiated in C1a material (Fig. 8c) and of debris flow DF2 initiated in IND material (Fig. 8d) without any calibration procedure.

Rheological parameters corresponding to the observed total solid fraction of the events (Malet et al., 2003a) were used as inputs values. The initial volume obtained by field measurements was set at 100 m^3 for the small mudflow and at 7700 m^3 for DF2. The discharge of the debris was expressed as a triangular hydrograph with a peak discharge of 10 m^3 s^{-1}. The preexisting channel bed topography is also given as input initial condition. The longitudinal path profile for both events was obtained from careful morphological and topometric survey. Outputs consist in the front location, the front velocity, the discharge regime and the variation of the flow thickness with time.

Results indicate that the runout code matches the observed geometry fairly well for the flow thickness and the runout distance (Fig. 8b). The relative error is less than 31% for the deposit thickness and less than 15% for the runout distance. This error is acceptable according to the relative error associated to the determination of the rheological parameters. In the depositional area, the shape of the deposits is also well reproduced (Fig. 8c,d). Moreover, compared to a previous modeling study, the relative error on the computed velocities is not much than 15% for the Cemagref 1-D code, as it may reach more than 1000% with the BING code (Malet et al., 2004a).

Therefore, as a good concordance between model predictions and reality has been observed, the Cemagref 1-D code can be used for hazard assessment.

7. Hazard assessment on the alluvial fan

The evaluation of hazard scenarios on alluvial fans is usually of primary interest in mountainous areas. This topic is particularly relevant in the Ubaye valley

where the hazard associated to such areas is particularly high, as suggested by historical events (van Beek and van Asch, 1996; Flageollet et al., 1999).

To prepare a hazard zonation (in terms of runout distance attained by the debris and deposit thickness), the following steps have been followed: (1) the estimation of the potential volume of debris needed to reach the apex of the alluvial fan and (2) the definition of the meteorological events able to initiate the failure of the corresponding volume of debris in the debris source area.

The methodology previously developed for the analysis of debris flow runout with the BING model has been used (Malet et al., 2004a). It consisted of performing several numerical simulations with the Cemagref 1-D code (1) by using the rheological and hydraulic parameters used in the debris flow mobility analysis, (2) by changing the volume of released sediment (the volume released at the beginning of the calculation corresponds to a volume of solid debris and water) and (3) by changing the total solid fraction (ϕ=0.40, ϕ=0.45 and ϕ=0.50). A peak discharge of 7 m^3 s^{-1} and a triangular hydrograph of 120 min are used in the simulations. These values, derived from the Crupedix methodology (Cemagref, 1980), correspond to a decenal flow discharge recurrence (Malet, 2003).

The longitudinal profile of the Sauze torrent was derived from a careful morphological mapping. More than 50 cross-sections were introduced in the model to take into account the narrowing and widening of the channel bed and reaches. In first approximation, no scouring of the channel and reaches due to the debris flow was considered.

We adjusted the volume of input debris with the assumption that the deposits must be at least 0.50 m thick. Usually, in case of debris flow accumulation, for hazard assessment and mapping (Shih et al., 1997; Petrascheck and Kienholz, 2003), this thickness corresponds to the minimum value at which the push prompting and damage effect on the exposed structures are effective. Fig. 9a shows the results of the scenario analysis. The lower horizontal axis shows the volume of sediment (solid debris+water) that propagated along the channel. For comparisons, the same graphical representation as used in Malet et al. (2004a) was used; the upper horizontal axis corresponds to the volume of solid debris for the different total solid fractions ϕ, assuming a failure of 15 m height and 60 m width in the source area, as observed for the DF1 and DF2 events.

For total solid fractions consistent with those generally observed in muddy debris flows (Coussot and Meunier, 1996), the minimal volume of sediment (mixture of debris and water) necessary to reach the apex ranges between 30,000 and 50,000 m^3 (Fig. 9a). Fig. 9b and c shows the geometry of the events. A maximum final deposit thickness of 0.51 and 0.44 m, respectively, are predicted by the model respectively on the apex and at the confluence. In the second case, even if the volume of released sediment is larger, the final deposits are finer because spreading occurs on the alluvial fan. The simulated velocities are consistent with those generally observed for muddy debris flows in the French Alps and lie in the range between 2 and 2.5 m s^{-1}.

Predictive seepage and stability analyses were then performed to estimate for which hydrological and mechanical conditions the release of such a volume is possible. Assuming a total solid fraction of ϕ=0.45, the volume of debris that has to fail in the debris source area ranges between 21,000 and 29,000 m^3. These estimations are consistent with those predicted with the simple BING model (18,000 to 25,000 m^3, Malet et al., 2004a).

Assuming a 60-m width and 15-m height failure in the debris source area, the slip surface must be located 23 to 30 m behind the secondary scarp. Assuming the cracked conditions of the seepage simulation (Fig. 7f), the meteorological events able to initiate a huge failure were investigated. The parametric analyses indicate that a rapid rise in groundwater level of about 1.0 m and a groundwater level of −0.20 m more or less parallel to the topographic surface would locate a slip surface 25 m behind the scarp and bring the F_s below 1. These hydrological conditions are attained for a cumulative input of water of 65 mm (over a 3-day-long period) corresponding to a 25-year return period rainfall.

Results of the stability and mobility analysis show therefore that realistic saturation conditions of the debris source area can trigger a long runout event. This simulation corresponds to the lower range of volumes needed to reach the fan. Indeed, scouring will add material to the debris flow during its course.

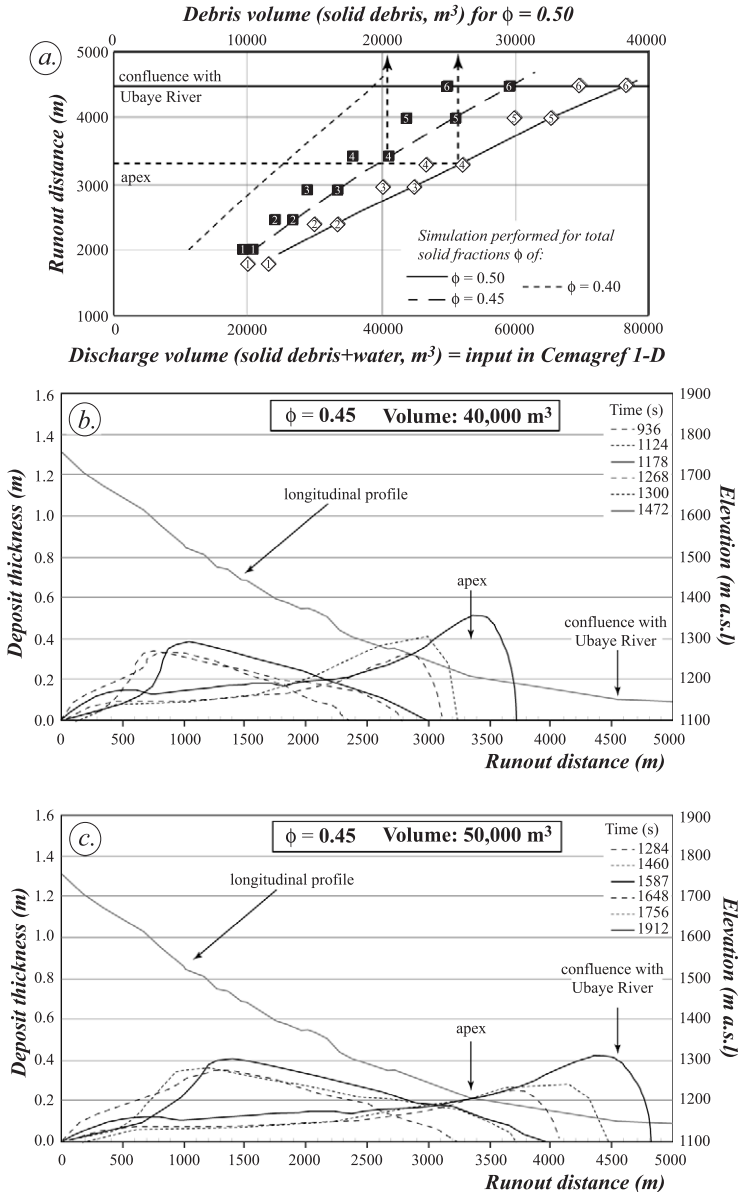

Fig. 9. Runout modeling scenarios for the Sauze alluvial fan. Estimation of the sediment volume needed to reach the apex of the torrent and the Ubaye river confluence for different total solid fractions (a). Simulated debris flow geometry at the apex (b) and at the Ubaye river confluence (c).

Some attention should also be given to the possibility of moisture content change with movement due to (1) the dissipation of the pore pressure due to the grain-size segregation and the development of a debris flow head consisting chiefly of gravel (Iverson, 2003) and (2) the dilution of the debris flow with surface water. With time, the surge may dilute or drain, and sorting may develop.

As proposed by Crosta (2001), the related risk could be ameliorated by zoning the torrential hazard

on the alluvial fan on the basis of deposit thickness by considering natural damming, obstruction of the river course, occlusion or destruction of bridges or damage to structures. This was not the focus of this study, but the work is actually in progress by using the two-dimensional debris flow spreading model developed by Laigle (1996) and validated on field events by Laigle et al. (2003).

8. Conclusion

Large landslides often show their complex nature through sudden changes in behaviour (from sliding to flowing) or in velocities (from less than 0.01 m day^{-1} over more than 1 m s^{-1}). These features are the cause of the high hazard associated with such landslides. The Super-Sauze case history is a good example of the possible evolution of landslides developed in clayey soils and allows the development and the validation of physically based models. Flow-like landslide hazard assessment is only relevant when field and laboratory studies are combined to numerical simulations (seepage model, stability model, runout model) on the basis of geomorphological assumptions. The proposed methodology allowed the evaluation of realistic risk scenarios for such instabilities.

A dynamic debris flow model has been used to estimate runout scenarios. The Cemagref 1-D code allows to represent the dynamics of the slurries without any use of parameter calibration. A good concordance between model predictions and reality has been observed. The simulated flow thickness, runout distance and velocities are concordant with the record of the real events.

Therefore, a parametric mobility analysis has shown that clayey earthflow can transform into 1-km runout debris flows (of volumes ranging between 2000 to 5000 m^3) under 5-year return period rainfall and into 4-km runout events (of volumes ranging between 30,000 and 50,000 m^3) under 25-year return period rainfall.

There is, nevertheless, a need for further development of analytical and modeling tools to properly address the transition from failure to postfailure stages for such complex landslides and to study the mechanisms, which may generate liquefaction. Major effort should also be put in the development of runout models able to take into account channel-bed scouring and variation of rheology with distance and time. Complex case studies, such as the Super-Sauze landslide, should be analysed in detail so as to provide a complete case history essential for the understanding of landslide induced debris flows.

Acknowledgements

This work was supported by grants from the French Ministry of Research under the ACI-CatNat contract Modélisation, Transformation, Ecoulement des Coulées boueuses dans les marnes (MOTE) and from the Centre National de la Recherche Scientifique under the INSU-PNRN contract ecoulement, contribution de laves Torrentielles dans les basins versants marneux (ECLAT). Contribution INSU N° 359. Contribution EOST N° 2004.01-UMR7516. The authors would like to thank S. Klotz, S. Pierre and A. Puissant for their precious help in the field in May 1999. We express our gratitude to Prof. F. M. Guadagno (Università del Sannio-Benevento, Italia) and to Prof. C. Kilburn (Benfield Greig Hazard Research Centre, University College London) for their constructive comments and suggestions. Prof. C. Ancey (Swiss Federal Institute of Technology, Lausanne) is kindly acknowledged for fruitful discussions on the rheology of natural clay-rich fluids.

References

Ancey, C., 2002. Debris flows and related phenomena. In: Balmforth, N., Provenzalle, A. (Eds.), Geomorphological Fluid Mechanics, Lecture Notes in Physics, vol. 582. Springer-Verlag, Berlin, pp. 528–547.

Antoine, P., Giraud, A., Meunier, M., Van Asch, Th.W.J., 1995. Geological and geotechnical properties of the "Terres Noires" in the southeastern France: weathering, erosion, solid transport and instability. Engineering Geology 40, 223–234.

Cemagref, 1980. Synthèse nationale sur les crues des petits bassins-versants. Méthodes Socose et Crupedix. Internal Report, Cemagref, Anthony, 120 pp.

Collinson, A.C., 2001. The cycle of instability: stress release and fissure flow as controls on gully head retreat. Hydrological Processes 15, 3–12.

Coussot, P., 1997. Mudflow Rheology and Dynamics. Balkema, Rotterdam. 272 pp.

Coussot, P., Ancey, C., 1999. Rhéophysique des pâtes et des suspensions. EDP Sciences, Paris. 266 pp.

Coussot, P., Meunier, M., 1996. Recognition, classification and mechanical description of debris flow. Earth-Science Reviews 40, 209–227.

Coussot, P., Proust, S., Ancey, C., 1996. Rheological interpretation of deposits of yield stress fluids. Journal of Non-Newtonian Fluid Mechanics 66, 55–70.

Crosta, G.B., 2001. Failure and flow development of a complex slide: the 1993 Sesa landslide. Engineering Geology 59, 173–199.

Edgers, L., Karlsrud, K., 1982. Soil flows generated by submarine slides—case studies and consequences. Norwegian Geotechnical Institute Publication 143, NGI, Oslo, 121p.

Fiorillo, F., Guadagno, F.M., Aquino, S., De Blasio, A., 2001. The December 1999 Cervinara landslides: further debris flows in the pyroclastic deposits of Campania (southern Italy). Bulletin of Engineering Geology and the Environment 60, 171–184.

Flageollet, J.-C., Maquaire, O., Weber, D., Martin, B., 1999. Landslides and climatic conditions in Barcelonnette and Vars Basin (southern Alps, France). Geomorphology 30, 65–78.

Flageollet, J.-C., Malet, J.-P., Maquaire, O., 2000. The 3-D structure of the Super-Sauze earthflow: a first stage towards modelling its behaviour. Physics and Chemistry of the Earth 25, 785–791.

Geo-Slope, 2000. SEEP/W/SLOPE/W. User Manual. Geo-Slope International, Calgary. 875 pp.

Harbitz, C.B., Issler, D., Keylock, C.J., 1998. Conclusions from a recent survey of avalanche computational models. Norwegian Geotechnical Institute Publication 203, NGI, Oslo. 225 pp.

Heim, A., 1932. Der Bergsturz von Elm. Deutsche Geologie Gesellschaft Zeitschrift 34, 74–115.

Henry, J.-B., Malet, J.-P., Maquaire, O., Grussenmeyer, P., 2002. The use of small format and low-altitude aerial photos for the realization of high-resolution DEMs in mountainous areas. Application to the Super-Sauze earthflow (Alpes-de-Haute-Provence, France). Earth Surface Processes and Landforms 27, 1339–1350.

Herschel, W.H., Bulkley, R., 1926. Measurement of consistency as applied to rubber–benzene solutions. American Society for Testing and Materials 26, 621–633.

Hungr, O., 1995. A model for the runout analysis of rapid flow slides, debris flows and avalanches. Canadian Geotechnical Journal 32, 610–623.

Hungr, O., Morgan, G.C., Kellerhals, R., 1984. Quantitative analysis of debris torrent hazards for the design of remedial measures. Canadian Geotechnical Journal 21, 663–677.

Hungr, O., Evans, S.G., Bovis, M.J., Hutchinson, J.N., 2001. A review of the classification of landslides of the flow type. Environmental and Engineering Geoscience 7, 221–238.

Hutchinson, J.N., 1988. Morphological and geotechnical parameters of landslides in relation to geology and hydrogeology. In: Bonnard, C. (Ed.), Landslides, Proceedings of the 5th International Symposium on Landslides, Lausanne. Balkema, Rotterdam, pp. 3–35.

Irgens, F., Norem, H., 1996. A discussion of the physical parameters that control the flow of natural landslides. In: Senneset, K. (Ed.), Landslides, Proceedings of the VIIth International Symposium on Landslides, Trondheim. Balkema, Rotterdam, pp. 1251–1256.

Iverson, R.M., 1997a. The physics of debris flow. Reviews of Geophysics 35, 245–296.

Iverson, R.M., 1997b. Hydraulic modeling of unsteady debris flow surges with solid–fluid interactions. In: Chen, C.-L. (Ed.), Proceedings of the 1st International Conference on Debris flow Hazards Mitigation, San Francisco. American Society of Civil Engineers, New York, pp. 550–560.

Iverson, R.M., 2003. The debris flow rheology myth. In: Rickenmann, D., Chen, C.-L. (Eds.), Proceedings of the 3rd International Conference on Debris flow Hazard Mitigation: Mechanics, Prediction and Assessment, Davos. Millpress, Rotterdam, pp. 303–314.

Iverson, R.M., Vallance, J.W., 2001. New views of granular mass flows. Geology 29, 115–118.

Iverson, R.M., Reid, M.E., LaHusen, R.G., 1997. Debris flow mobilization from landslides. Annual Reviews: Earth and Planetary Sciences 25, 85–138.

Jenkinson, A.F., 1955. The frequency distribution of the annual maximum (or minimum) values of meteorological elements. Quarterly Journal of the Royal Meteorological Society 81, 158–171.

Johnson, A.M., Rodine, J.R., 1984. Debris flow. In: Brunsden, D., Prior, D.B. (Eds.), Slope Instability. Wiley, Chichester, pp. 257–362.

Klubertanz, G., Laloui, L., Vulliet, L., 2000. Parameters governing debris flow initiation. In: Wieczorek, G.F., Naeser, N.D. (Eds.), Proceedings of the 2nd International Conference on Debris flow Hazards Mitigation, Taipei. Balkema, Rotterdam, pp. 73–79.

Laigle, D., 1996. Two-dimensional modelling of debris flow spreading on alluvial fans. In: Müller, A. (Ed.), Proceedings of the 2nd International Conference on Hydroinformatics, Zürich. Balkema, Rotterdam, pp. 651–657.

Laigle, D., Coussot, P., 1997. Numerical modelling of debris flows. Journal of Hydraulic Engineering 123, 617–623.

Laigle, D., Marchi, L., 2000. Example of mud/debris flow hazard assessment using numerical models. In: Wieczorek, G.F., Naeser, N.D. (Eds.), Proceedings of the 2nd International Conference on Debris-flow Hazard Mitigation: Mechanics, Prediction and Assessment, Taipeh. Balkema, Rotterdam, pp. 260–269.

Laigle, D., Hector, A.-F., Hübl, J., Rickenmann, D., 2003. Comparison of numerical simulation of muddy debris flow spreading to records of real events. In: Rickenmann, D., Chen, C.-L. (Eds.), Proceedings of the 3rd International Conference on Debris flow Hazard Mitigation: Mechanics, Prediction and Assessment, Davos. Millpress, Rotterdam, pp. 635–646.

Lambe, T.W., Whitman, R.V., 1979. Soil Mechanics. Wiley, New York. 553 p.

LeMignon, G., Cojean, R., 2002. Rôle de l'eau dans la mobilisation de glissement-coulées (Barcelonnette, France). In: Rybar, J., Stemberk, J., Wagner, P. (Eds.), Landslides, Proceedings of the 1st European Conference on Landslides, Prague. Swets and Zeitlinger Publishers, Lisse, pp. 239–244.

Locat, J., Lee, H.J., Nelson, C.H., Schwab, W.C., Twichell, D.C., 1996. Analysis of the mobility of far reaching debris flows on the Mississippi Fan, Gulf of Mexico. In: Senneset, K. (Ed.),

Landslides, Proceedings of the VIIth International Symposium on Landslides, Trondheim. Balkema, Rotterdam, pp. 555–560.
Major, J.J., Pierson, T.C., 1992. Debris flow rheology: experimental analyses of fine-grained slurries. Water Resources Research 28, 841–857.
Malet, J.-P., Maquaire, O., Calais, E., 2002a. The use of global positioning system for the continuous monitoring of landslides. Application to the Super-Sauze earthflow (Alpes-de-Haute-Provence, France). Geomorphology 43, 33–54.
Malet, J.-P., Remaître, A., Ancey, C., Locat, J., Meunier, M., Maquaire, O., 2002b. Caractérisation rhéologique des coulées de débris et laves torrentielles du bassin marneux de Barcelonnette (Alpes-de-Haute-Provence, France). Premiers résultats. Rhéologie 1, 17–25.
Malet, J.-P., 2003. Les glissements de type écoulement dans les marnes noires des Alpes du Sud. Morphologie, fonctionnement et modélisation hydro-mécanique. Doctoral thesis in Earth Science, Louis Pasteur University, Strasbourg, 394 pp.
Malet, J.-P., Remaître, A., Maquaire, O., Ancey, C., Locat, J., 2003a. Flow susceptibility of heterogeneous marly formations. Implications for torrent hazard control in the Barcelonnette basin (Alpes-de-Haute-Provence, France). In: Rickenmann, D., Chen, C.-L. (Eds.), Proceedings of the Third International Conference on Debris flow Hazard Mitigation: Mechanics, Prediction and Assessment, Davos, Switzerland. Millpress, Rotterdam, pp. 351–362.
Malet, J.-P., Auzet, A.-V., Maquaire, O., Ambroise, B., Descroix, L., Estèves, M., Vandervaere, J-P., Truchet, E., 2003b. Investigating the influence of soil surface features on infiltration on marly hillslopes. Application to Callovo–Oxfordian black marls slopes in the Barcelonnette basin (Alpes-de-Haute-Provence, France). Earth Surface Processes and Landforms 28, 547–564.
Malet, J.P., Maquaire, O., Locat, J., Remaître, A., 2004a. Assessing debris flow hazards associated with slow-moving landslides: methodology and numerical analyses. Landslides 1, 83–90.
Malet, J.-P., Laigle, D., Locat, J., Remaître, A., Maquaire, O., 2004b. Cross-validation of two debris flows run out models on a clay-shale catchment of Southeast France. In: Lacerda, W.A., Ehrlich, M., Fontura, S.A.B., Sayâo, A.S.F. (Eds.), Proceedings of the 9th International Symposium on Landslides, Rio de Janeiro, Brazil. Balkema, Leiden, pp. 1367–1373.
Malet, J.-P., van Asch, Th.W.J., van Beek, R., Maquaire, O. (in review). Dynamic hydrological modelling of a fast moving complex landslide in the French Alps. Hydrological Processes, 18p (submitted for publication).
Maquaire, O., Flageollet, J.-C., Malet, J.-P., Schmutz, M., Weber, D., Klotz, S., Albouy, Y., Descloîtres, M., Dietrich, M., Guérin, R., Schott, J.-J., 2001. Une approche multi-disciplinaire pour la connaissance d'un glissement-coulée dans les marnes noires (Super-Sauze, Alpes-de-Haute-Provence, France). Revue Française de Géotechnique 95/96, 15–31.
Maquaire, O., Malet, J.-P., Remaître, A., Locat, J., Klotz, S., Guillon, J., 2003. Instability conditions of marly hillslopes, towards landsliding or gullying? The case of the Barcelonnette basin, south east France. Engineering Geology 70, 109–130.
O'Brien, J.S., Julien, P.Y., 1988. Laboratory analyses of mudflow properties. Journal of Hydraulic Engineering 114 (8), 877–887.
O'Brien, J.S., Julien, P.J., Fullerton, W.T., 1993. Two-dimensional water flood and mudflow simulation. Journal of Hydraulic Engineering 119, 244–261.
Petrascheck, A., Kienholz, H., 2003. Hazard assessment and mapping of mountain risks in Switzerland. In: Rickenmann, D., Chen, C.-L. (Eds.), Proceedings of the 3rd International Conference on Debris flow Hazards Mitigation, Davos. Millpress, Rotterdam, pp. 25–39.
Picarelli, L., 2001. Transition from slide to earthflow and the reverse. In: Sassa, K. (Ed.), Transition from Slide to Flow. Mechanisms and Remedial Measures, Proceedings of the Conference, Trabzon, pp. 21–54.
Pierson, T., Costa, J.E., 1987. A rheologic classification of subaerial sediment-water flows. In: Costa, J.E., Wieczorek, G.F. (Eds.), Debris flows/Avalanches: Process, Recognition and Mitigation, Geological Society of American Review of Engineering Geology, vol. 7, pp. 1–12.
Richards, A.L., 1931. Capillary conductivity of liquid through porous media. Physics 1, 316–333.
Rickenmann, D., 1999. Empirical relationships for debris flows. Natural Hazards 19, 47–77.
Rickenmann, D., Koch, T., 1997. Comparison of debris flow modelling approaches. In: Chen, C.-L. (Ed.), Proceedings of the 1st International Conference on Debris flow Hazards Mitigation, San Francisco. American Society of Civil Engineers, New-York, pp. 576–584.
Scheidegger, A.E., 1973. On the prediction of the reach and velocity of catastrophic landslides. Rock Mechanics 5, 231–236.
Shih, B.J., Shieh, C.L., Chen, L.J., 1997. The grading of risk for hazardous debris flow zones. In: Chen, C.-L. (Ed.), Proceedings of the 1st International Conference on Debris flow Hazards Mitigation, San Francisco. American Society of Civil Engineers, New York, pp. 219–228.
Suhayda, J.N., Prior, D.B., 1979. Application of infinite slope analysis to submarine sediment instabilities, Mississippi Delta. Engineering Geology l4, 1–10.
Takahashi, T., 1991. Debris Flows. Balkema, Rotterdam, 165 pp.
van Beek, L.P.H., van Asch, T.W.J., 1996. The mobility characteristics of the La Valette landslide. In: Senneset, K. (Ed.), Landslides, Proceedings of the VIIth International Symposium on Landslides, Trondheim. Balkema, Rotterdam, pp. 1417–1421.
Vaunat, J., Leroueil, S., 2002. Analysis of post-failure slope movements within the framework of hazard and risk analysis. Natural Hazards 26, 83–109.